Effects of temperature dependence of electrical and thermal conductivities on the Joule heating of a one dimensional conductor

F. Antoulinakis, D. Chernin, Peng Zhang, and Y. Y. Lau

Citation: Journal of Applied Physics **120**, 135105 (2016); doi: 10.1063/1.4964112
View online: http://dx.doi.org/10.1063/1.4964112
View Table of Contents: http://aip.scitation.org/toc/jap/120/13
Published by the American Institute of Physics

JOURNAL OF APPLIED PHYSICS **120**, 135105 (2016)

Effects of temperature dependence of electrical and thermal conductivities on the Joule heating of a one dimensional conductor

F. Antoulinakis,[1] D. Chernin,[2] Peng Zhang,[1,a)] and Y. Y. Lau[1]
[1]*Department of Nuclear Engineering and Radiological Sciences, The University of Michigan, Ann Arbor, Michigan 48109, USA*
[2]*Leidos, Inc., Reston, Virginia 20190, USA*

(Received 4 August 2016; accepted 20 September 2016; published online 5 October 2016)

We examine the effects of temperature dependence of the electrical and thermal conductivities on Joule heating of a one-dimensional conductor by solving the coupled non-linear steady state electrical and thermal conduction equations. The spatial temperature distribution and the maximum temperature and its location within the conductor are evaluated for four cases: (i) constant electrical conductivity and linear temperature dependence of thermal conductivity, (ii) linear temperature dependence of both electrical and thermal conductivities, (iii) the Wiedemann–Franz relation for metals, and (iv) polynomial fits to measured data for carbon nanotube fibers and for copper. For (i) and (ii), it is found that there are conditions under which no steady state solution exists, which may indicate the possibility of thermal runaway. For (i), analytical solutions are constructed, from which explicit expressions for the parameter bounds for the existence of steady state solutions are obtained. The shifting of these bounds due to the introduction of linear temperature dependence of electrical conductivity (case (ii)) is studied numerically. These results may provide guidance in the design of circuits and devices in which the effects of coupled thermal and electrical conduction are important. *Published by AIP Publishing*. [http://dx.doi.org/10.1063/1.4964112]

I. INTRODUCTION

Joule heating limits the operation of most current carrying components and devices, ranging from large high power systems to nanoscale wires and devices. The coupled thermal-electrical conduction problem is important for wire-array Z-pinches,[1] power transmission lines,[2] high power microwave devices,[3,4] and electrical contacts.[5–9] In a Z-pinch, in particular, coupled thermal-electrical conduction is responsible for an electrothermal instability.[10]

Recent advancements in nanotechnology, the miniaturization of electronic devices, and the increase in density of circuit integration make Joule heating increasingly important to device performance and lifetime. The growing packing density and the power consumption of very large scale integration (VLSI) circuits, in particular, have made thermal effects one of the most important concerns of VLSI designers.[11] In micro-electro-mechanical (MEM) switches, the durability of the devices is largely limited by Joule heating at the contacting asperities.[12,13] Coupled thermal-electrical effects play important roles in current emission performance as well as the stability of carbon nanofiber based field emitters.[14–17] There has also been interest in understanding and controlling the local temperature increases within electrically driven nanoscale wires and metallic interconnects.[18] Thermal stability is one of the key challenges in nanoscale devices made of novel materials, such as graphene[19–21] and organic materials.[22,23] In electrically pumped nanolasers for chip-scale optical communications, thermal management is of crucial importance to realize room temperature operation.[24,25]

Available 3D finite element simulation codes may be used to compute the effects of coupled electrical and thermal conduction with great accuracy. However, the parametric dependences of the solution are difficult to determine from such purely numerical calculations. Here, by using a very simple 1D model, we aim to provide a better understanding of the underlying physics and the influences of multiple parameters on key properties of the solution, including the maximum temperature and its location in the conductor.

In this paper, we evaluate the effects of temperature dependence of the electrical and thermal conductivities on the Joule heating of a one-dimensional (1D) conductor, by solving the coupled non-linear steady state electrical and thermal conduction equations. Section II provides the formulation of our simple theory. Results and discussions are given in Section III, where we have analyzed four cases: (1) constant electrical conductivity and linear temperature dependent thermal conductivity, (2) linear temperature dependence of both electrical and thermal conductivities, (3) the Wiedemann–Franz (WF) law, and (4) realistic examples for carbon nanotube fibers (CNFs) and copper. A summary and suggestions for future research are given in Section IV.

II. FORMULATION

Consider a one-dimensional (1D) conductor of length L, which is held at temperatures T_1 and T_2 at its ends, and across which a voltage of V_0 is applied. The steady state heat conduction and electrical current continuity equations are, respectively,

a)Present Address: Department of Electrical and Computer Engineering, Michigan State University, East Lansing, Michigan 48824-1226, USA. Electronic mail: pz@egr.msu.edu

$$\frac{d}{dz}\left(\kappa(T,z)\frac{d}{dz}T(z)\right)+\sigma(T,z)\left(\frac{d}{dz}V(z)\right)^2=0, \quad (1)$$

$$\frac{d}{dz}\left(\sigma(T,z)\frac{d}{dz}V(z)\right)=0, \quad (2)$$

where $\kappa(T,z)$ and $\sigma(T,z)$ are the temperature-dependent thermal and electrical conductivities, respectively, and $V(z)$ is the potential, $T(z)$ is the temperature, and z is the location along the 1D conductor. The above equations are solved with the following boundary conditions:

$$T(z=0)=T_1, \quad (3a)$$

$$T(z=L)=T_2, \quad (3b)$$

$$\phi(z=0)=0, \quad (3c)$$

$$\phi(z=L)=V_0. \quad (3d)$$

Combining Eqs. (1), (2), (3c), and (3d), we have

$$\frac{d}{dz}\left(\kappa(T,z)\frac{dT}{dz}\right)+\frac{J_c^2}{\sigma(T,z)}=0, \quad (4)$$

where $J_c=\sigma dV/dz=$ constant is the current density in the conductor, which satisfies $\int_0^L (J_c/\sigma)dz=V_0$.

For simplicity, we introduce the normalizations, $\bar{z}=z/L$, $\bar{T}=(T-T_1)/T_0$, with $T_0=T_1$ if $T_1=T_2$, and $T_0=T_2-T_1$ if $T_1\neq T_2$, $\bar{V}=V/V_0$, $\bar{\kappa}(\bar{T},\bar{z})=\kappa(T,z)/\kappa_0$, $\bar{\sigma}(\bar{T},\bar{z})=\sigma(T,z)/\sigma_0$, $\alpha=\sigma_0 V_0^2/\kappa_0 T_0$, $J_0=\sigma_0 V_0/L$, and $\overline{J_c}=J_c/J_0$. Note that the parameter α includes the information about the boundary conditions in Eqs. (3a)–(3d). κ_0 and σ_0 are constants to be defined below. Equation (4) becomes

$$\frac{d}{d\bar{z}}\left(\bar{\kappa}\frac{d\bar{T}}{d\bar{z}}\right)=-\alpha\frac{\overline{J_c}^2}{\bar{\sigma}}, \quad (5)$$

where $\overline{J_c}\int_0^1 d\bar{z}/\bar{\sigma}=1$, and the boundary conditions (Eqs. (3a) and (3b)) are

$$\bar{T}(\bar{z}=0)=0, \quad (6a)$$

$$\bar{T}(\bar{z}=1)=\begin{cases}0, & \text{if } T_1=T_2,\\ 1, & \text{if } T_1\neq T_2.\end{cases} \quad (6b)$$

Equations (5) and (6) are solved to give the steady-state solution for the coupled electrical-thermal conduction. In principle, they can be solved numerically for arbitrary temperature dependence of electrical conductivity $\bar{\sigma}(\bar{T},\bar{z})$ and thermal conductivity $\bar{\kappa}(\bar{T},\bar{z})$. We focus on several special cases that can be of practical importance. Note that if $T_1>T_2$, we have $T_0<0$, which means that decreasing (increasing) normalized temperature $\bar{T}$ gives increasing (decreasing) absolute temperature T.

III. RESULTS AND DISCUSSION

Case 1: Constant electrical conductivity and linear temperature dependent thermal conductivity

For the special case of constant electrical conductivity, $\sigma=\sigma_0$, and linear temperature dependence of thermal conductivity, $\kappa=\kappa_0+\kappa'(T-T_1)$, we have $\bar{\sigma}=1$ and $\bar{\kappa}=1+\eta\bar{T}$, with $\eta=\kappa' T_0/\kappa_0$. Note that η specifies the slope of the temperature dependence of the thermal conductivity for given boundary temperatures. This case may not sufficiently approximate physical materials in necessarily large temperature range, but it can be solved analytically to give a basic understanding of our model. Solving Eqs. (5) and (6) gives

$$\bar{T}(\bar{z})=\begin{cases}\dfrac{-1+\sqrt{\alpha\eta\bar{z}(1-\bar{z})+1}}{\eta} & \text{if } T_1=T_2;\\ \dfrac{-1+\sqrt{-\eta\alpha\bar{z}^2+\eta(\alpha+\eta+2)\bar{z}+1}}{\eta} & \text{if } T_1\neq T_2.\end{cases} \quad (7a,b)$$

For the case of $T_1=T_2$, the temperature distribution along the 1D conductor from Eq. (7a) is plotted in Fig. 1(a), for various values of α and η. The maximum temperature $\bar{T}_{max}$ is

$$\bar{T}_{max}=\frac{-1+\sqrt{\alpha\eta/4+1}}{\eta}, \qquad \text{if } T_1=T_2, \quad (8)$$

which always occurs at the center of the 1D conductor $\bar{z}_{max}=0.5$, as seen from Fig. 1(a). However, it is important to note that the solution in Eq. (7a) becomes unphysical when $\alpha\eta<-4$. This happens when $\bar{T}$ becomes such that $\bar{\kappa}<0$ at some location (e.g., $\bar{z}_{max}$) of the 1D conductor. We note that the absence of a steady state solution may or may not indicate thermal runaway.[26]

For the case of $T_1\neq T_2$, the temperature distribution along the 1D conductor from Eq. (7b) is plotted in Fig. 1(b), for various values of α and η. When $T_1\neq T_2$, the maximum temperature is found from Eq. (7b) to be

$$\bar{T}_{max}=\begin{cases}\dfrac{-1+\sqrt{\left(\frac{\eta}{4\alpha}\right)(\alpha+\eta+2)^2+1}}{\eta}, & \text{if } (\eta+2)<|\alpha|, \text{ if } T_1\neq T_2\\ 1(\text{when } T_1<T_2),\ 0(\text{when } T_1>T_2), & \text{otherwise},\end{cases} \quad (9a,b)$$

which occurs at $\bar{z}_{max}=(\alpha+\eta+2)/\alpha$ when $\alpha(\eta+2)<\alpha^2$, and at $\bar{z}_{max}=0$ or 1 otherwise. In the last case, the temperature range along the 1D conductor is bounded by the temperature at two ends, $[T_1,T_2]$.

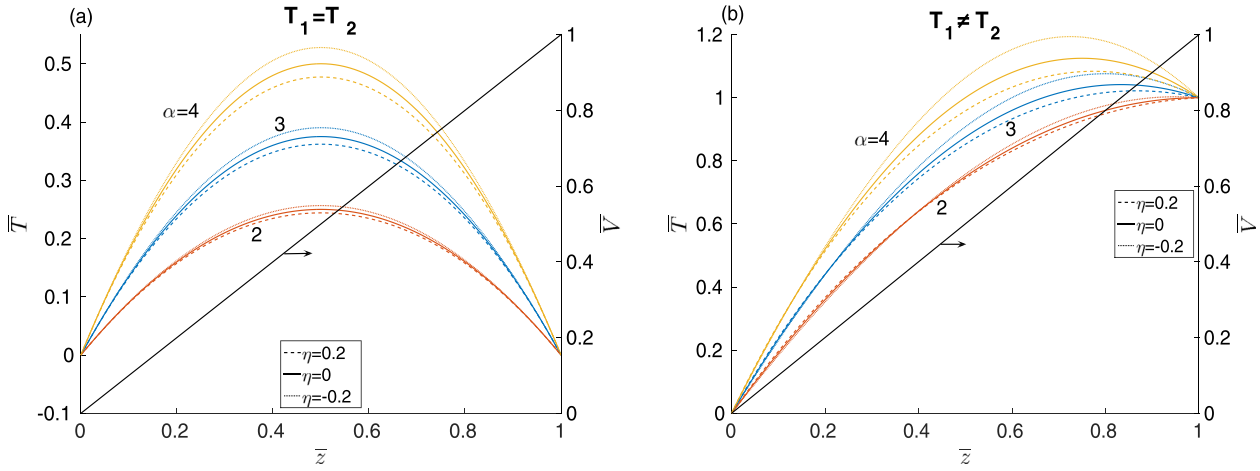

FIG. 1. Steady state solution $\bar{T}(\bar{z})$ and $\bar{V}(\bar{z})$ for (a) $T_1 = T_2$ from Eq. (7a), and (b) $T_1 \neq T_2$ from Eq. (7b), for various values of α and η in Case 1.

For $T_1 \neq T_2$, the conditions for the existence of physical steady-state solution in Eq. (7b) are

$$\alpha \leq -\frac{(\eta+2)^2}{\eta}, \qquad if\ -1 \leq \eta < 0, \tag{10a}$$

$$\alpha \geq -\frac{(\eta+2)^2}{\eta}, \qquad if\ \eta > 0. \tag{10b}$$

These conditions are plotted in Fig. 2, where the "Lower Bound" corresponds to (10a) and "Bounds" to (10b). Within the bounds shown (grey area), it is ensured that $\overline{\kappa} > 0$ for all points along the 1D conductor. Outside the boundaries of existence of solution in Fig. 2, $\overline{\kappa}$ becomes imaginary at certain location in z. Possible resulting time-dependent solutions include thermal runaway, oscillation, or non-periodic, bounded variation in time. Our model so far does not answer the question of which one occurs. These issues will be studied in the future. Note that in the limit of $\eta \to 0$, the RHS of Eq. (10) becomes $-(\eta+2)^2/\eta \to -4/\eta$, which is the bound for the case of $T_1 = T_2$ (2nd sentence after Eq. (8)). This is expected since $\eta \to 0$ indicates $T_0 = T_2 - T_1 \to 0$; thus, the solution asymptotically approaches that of $T_1 = T_2$. In the opposite limit of $\eta \to \infty$, $-(\eta+2)^2/\eta \to -\eta$, the bound approaches $\alpha \geq -\eta$ asymptotically.

Note that as long as the electrical conductivity is a constant, $\bar{\sigma} = 1$, the current $\overline{J_c} = 1$ is independent of the temperature in the conductor. Thus, the potential profile is always $\bar{V}(\bar{z}) = \bar{z}$, for both cases of $T_1 = T_2$ and $T_1 \neq T_2$, as shown in Fig. 1.

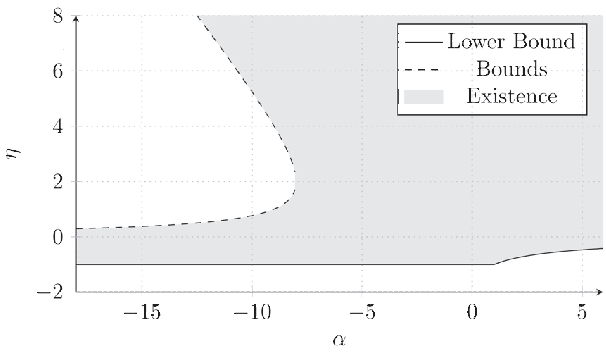

FIG. 2. Bounds for the existence of steady-state solution for Case 1 with $T_1 \neq T_2$.

Case 2: Linear temperature dependence of both electrical and thermal conductivities

In this case, we assume both electrical and thermal conductivities have linear temperature dependence, $\sigma = \sigma_0 + \sigma'(T - T_1)$ and $\kappa = \kappa_0 + \kappa'(T - T_1)$. After normalization, we have $\bar{\sigma} = 1 + \xi\bar{T}$ and $\bar{\kappa} = 1 + \eta\bar{T}$, with $\xi = \sigma' T_0/\sigma_0$ and $\eta = \kappa' T_0/\kappa_0$. Since analytical treatments are no longer available, Equations (5) and (6) are solved numerically. In the numerical calculation, the values of $\frac{d\bar{T}}{d\bar{z}}|_{\bar{z}=0}$ and $\bar{J}$ are found iteratively until the correct boundary conditions are met.

As in Case 1, there exist bounds beyond which there is no steady state solution for Eqs. (5) and (6). These bounds are found numerically by scanning α and η for a given ξ. The results are shown in Fig. 3 for different values of ξ, for both $T_1 = T_2$ and $T_1 \neq T_2$. Note that now solutions do not exist when either $\bar{\kappa} < 0$ or $\bar{\sigma} < 0$. However, we limit the range of our numerical calculation to only track down the lack of solutions because of $\bar{\kappa} < 0$ only, in order to compare the shifts of the bounds with respect to those in Case 1. As seen in Fig. 3, the lower bounds experience an upper left (lower right) shift for increasing (decreasing) value of ξ for both $T_1 = T_2$ and $T_1 \neq T_2$, whereas the upper bounds (which only exist for the case $T_1 \neq T_2$) experience an upper right shift. That is, all the bounds shift towards $\alpha = 0$ as ξ increases. As we shall see later (Fig. 5), increasing ξ will increase the maximum temperatures in the conductor; thus, $|\alpha|$ has to be reduced in order to decrease the rate of Joule heating (cf. Eq. (5)) to ensure the existence of a steady state solution. Note that the bounds for $\xi = 0$ in Fig. 3(b) are identical to those in Fig. 2.

The temperature and electric potential distribution along the 1D conductor calculated from Eqs. (5) and (6) is shown in Figs. 4(a) and 4(b), for various values of α and ξ with $\eta = 0$. As ξ increases, the maximum temperature increases. For $T_1 = T_2$, the maximum temperature always occurs at the center of the conductor $\bar{z} = 0.5$. For $T_1 \neq T_2$, the position where maximum temperature occurs shifts towards $\bar{z} = 0.5$ as ξ increases. (See Figs. 5 and 6 for further details on these

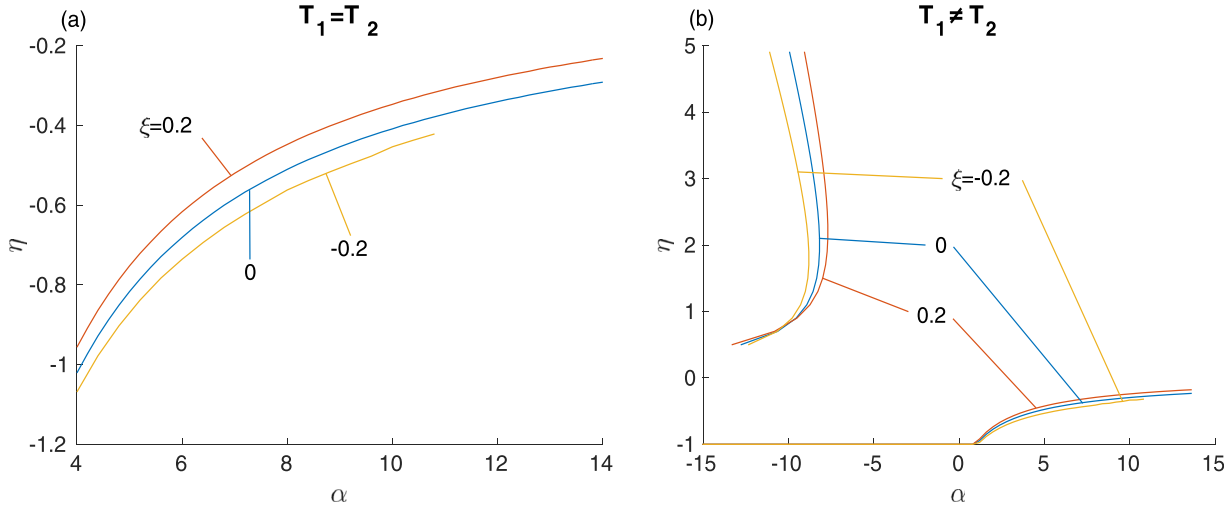

FIG. 3. Bounds for the existence of steady-state solution for case 2 with (a) $T_1 = T_2$ and (b) $T_1 \neq T_2$, for various values of ξ.

quantities.) The normalized potential profile $\bar{V}(\bar{z})$ is not sensitive to α or η. For a given α, the current $\overline{J_c}$ is plotted as a function of ξ, for various values of α in Figs. 4(c) and 4(d). The value of $\overline{J_c}$ increases with ξ. For $\xi > 0$, $\overline{J_c}$ increases as α increases, whereas for $\xi < 0$, $\overline{J_c}$ decreases as α increases.

The maximum temperature $\bar{T}_{max}$ is calculated numerically for different values of α, η, and ξ, as shown in Fig. 5. In all the cases, we can see that $|T_{max}|$ decreases as η increases; this is because the increasing thermal conductivity $\bar{\kappa}$ will make the generated heat conducted away more easily. $|T_{max}|$ increases as $|\alpha|$ increases, since the rate of heating increases with $|\alpha|$ (cf. Eq. (5)). It is also clear that $|T_{max}|$ increases as ξ increases, since the current (thus the power) will increase in the conductor because of larger electrical conductivity $\bar{\sigma}$.

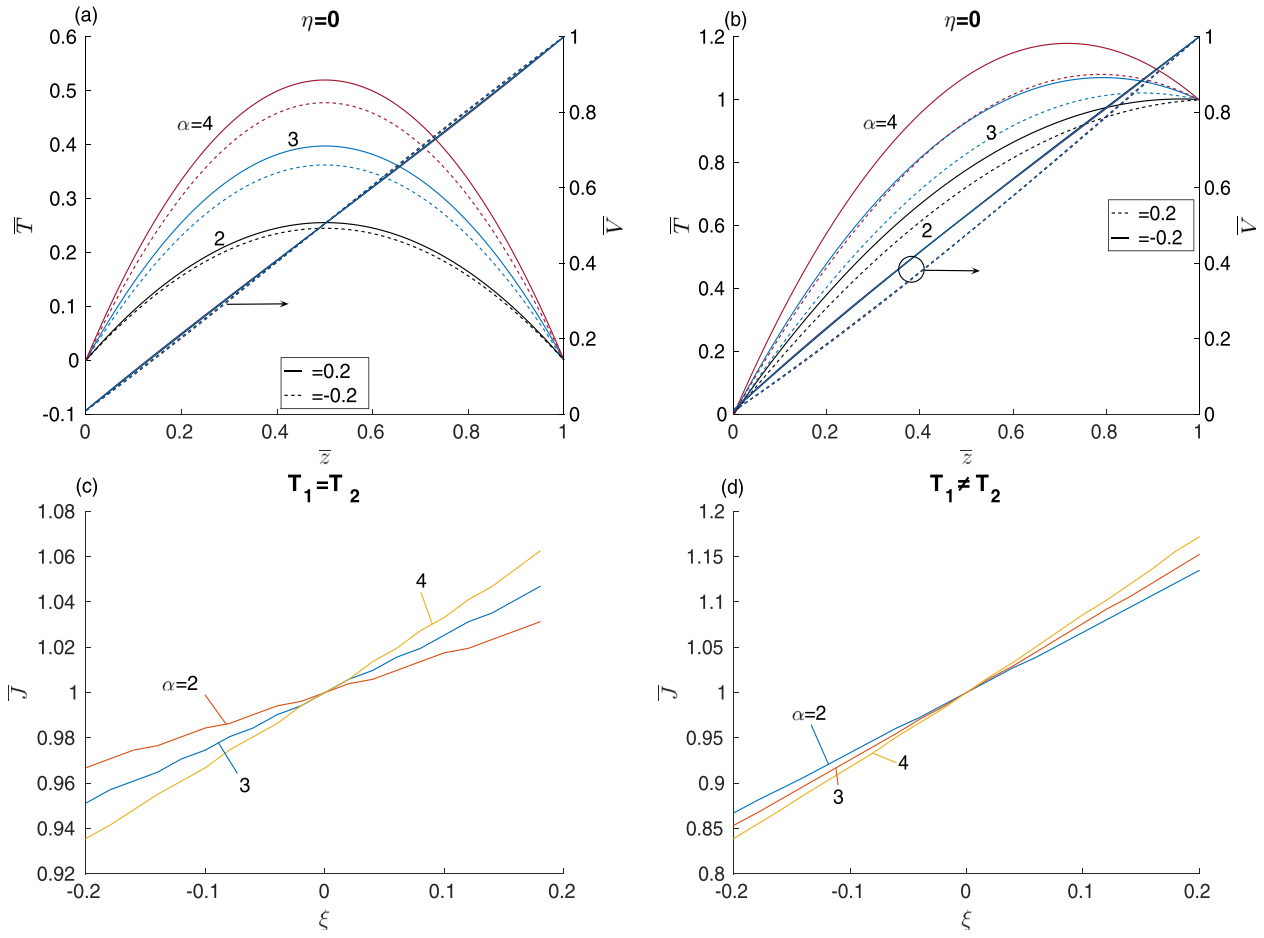

FIG. 4. Steady state solution $\bar{T}(\bar{z})$ and $\bar{V}(\bar{z})$ obtained from Eqs. (5) and (6) for (a) $T_1 = T_2$ and (b) $T_1 \neq T_2$, for various values of α and ξ for $\eta = 0$. The corresponding current $\overline{J_c}$ as a function of ξ for (c) $T_1 = T_2$ and (d) $T_1 \neq T_2$.

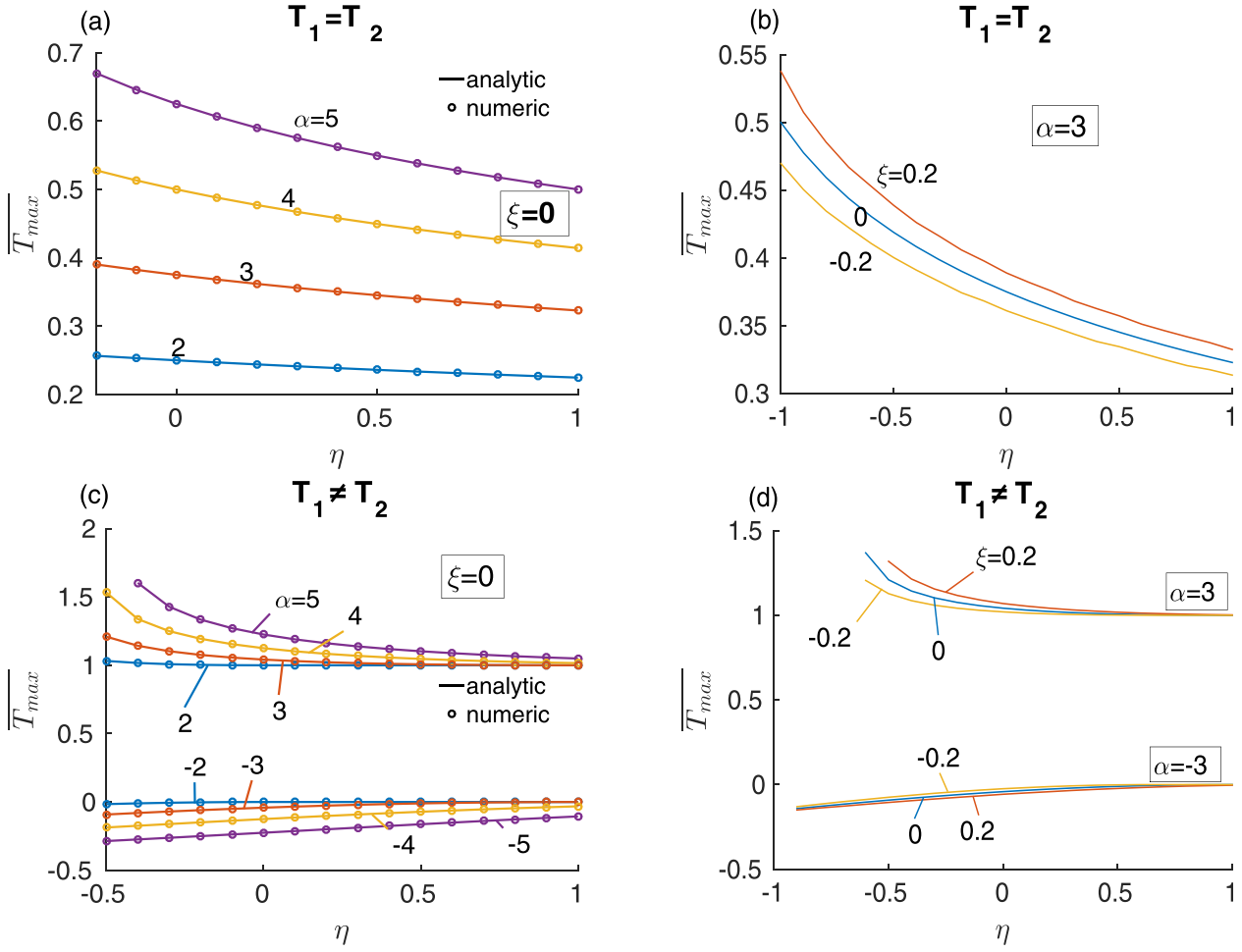

FIG. 5. Maximum temperature $\bar{T}_{max}$ for various values of α and $\xi = 0$ (left) and for various values of ξ and $\alpha = \pm 3$ (right). Both the cases, $T_1 = T_2$ (top) and $T_1 \neq T_2$ (bottom) were plotted. The lines in (a) and (c) are from Eqs. (8) and (9), respectively, and the symbols are from numerical calculation.

Note that negative values of α correspond to $T_2 < T_1$. For the special case of $\xi = 0$, the numerical calculations in Figs. 5(a) and 5(c) give almost identical results obtained analytically from Eqs. (8) and (9).

For $T_1 = T_2$, the maximum temperature always occurs at $\bar{z}_{max} = 0.5$ because of symmetry. For $T_1 \neq T_2$, we plot $\bar{z}_{max}$ vs η in Fig. 6. It is apparent that $\bar{z}_{max}$ is located in the region of $0 \leq \bar{z}_{max} < 0.5$ when $\alpha < 0$ (i.e., $T_1 > T_2$), and within $0.5 < \bar{z}_{max} \leq 1$ when $\alpha > 0$ (i.e., $T_1 < T_2$). $\bar{z}_{max}$ becomes closer to 0.5 (the center) as $|\alpha|$ increases. Also, $\bar{z}_{max}$ becomes closer to 0.5 when either η decreases or ξ increases.

For the special case $\xi = 0$, the numerically obtained $\bar{z}_{max}$ gives almost identical results from the analytical solution, where $\bar{z}_{max}$ $(\neq 0, 1)$ is a linear function of η.

Case 3: Wiedemann–Franz law

The Wiedemann–Franz (WF) law[6,27] is a relation between the thermal and electrical conductivity of metals of the form

$$\frac{\kappa}{\sigma} = lT, \tag{11}$$

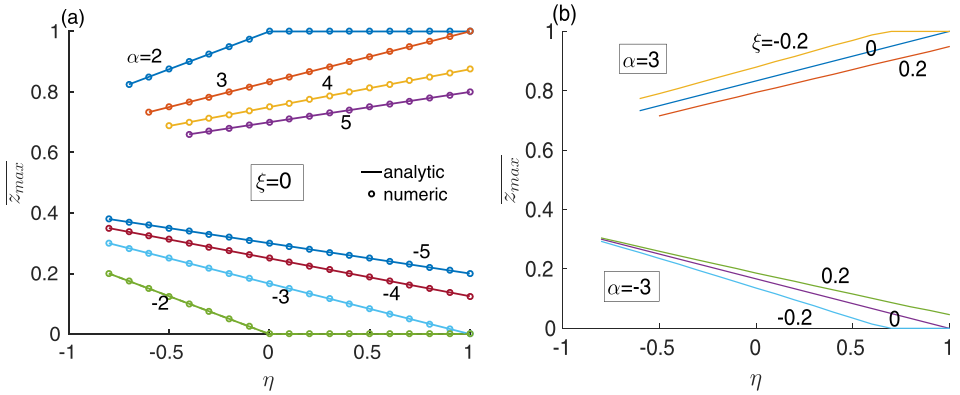

FIG. 6. Location of maximum temperature for various values of α and $\xi = 0$ (left) and for various values of ξ and $\alpha = \pm 3$ (right) for $T_1 \neq T_2$. The lines in (a) are from analytical calculation, and the symbols are from numerical calculation.

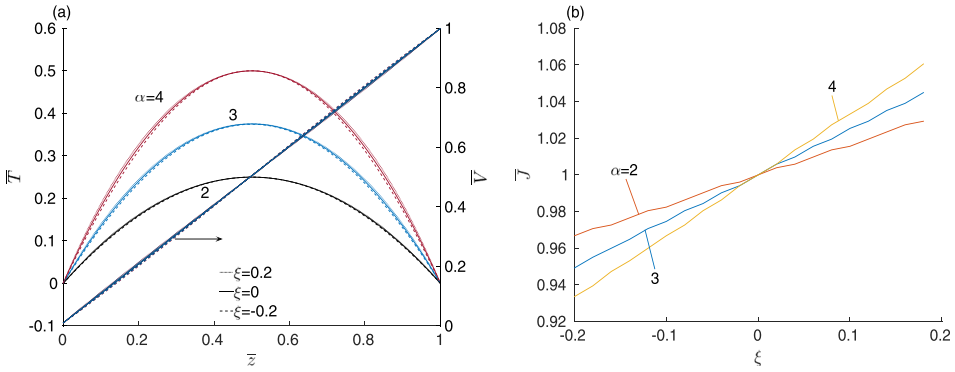

FIG. 7. Steady state solution (a) $\bar{T}(\bar{z})$ and $\bar{V}(\bar{z})$, and (b) $\overline{J_c}$ obtained from Eqs. (5) and (6) for $T_1 = T_2$ with Wiedemann-Franz law assumed.

where $l \approx 2.44 \times 10^{-8}\,\mathrm{W\,\Omega\,K^{-2}}$ is the Lorenz number. Further discussion on the application of WF law to various materials may be found at Refs. 27–30. For simplicity, we consider only the special case of $T_1 = T_2$ with linear temperature dependence of electrical conductivity, $\bar{\sigma} = 1 + \xi\bar{T}$. Using the same normalization as in Section II, Eq. (11) becomes

$$\bar{\kappa} = (1 + \bar{T})\bar{\sigma}, \tag{12}$$

where we have used $\kappa_0/\sigma_0 = lT_1$, with $\alpha = V_0^2/lT_1^2$. Using Eq. (12), Eqs. (5) and (6) may be solved numerically. The temperature and electrical potential distributions are shown in Fig. 7(a), for various values of α and ξ. It is notable that a change in the value of ξ does not change the temperature and potential profiles significantly or the maximum temperature. The constant current $\overline{J_c}$ is plotted as a function of ξ, for various values of α in Fig. 7(b). The behavior of $\overline{J_c}$ is similar to Case 2 with linear temperature dependence of σ and κ, as σ is modeled the same way and the temperature profile does not vary significantly.

Figure 8 shows the maximum temperature does not depend on ξ but only on α. If the WF law holds, it is possible to find an analytical solution for the maximum temperature (see Appendix)

$$\overline{T_{max}} = \sqrt{1 + \frac{\alpha}{4}} - 1, \tag{13}$$

which is independent of $\bar{\sigma}(\bar{T})$ and $\bar{\kappa}(\bar{T})$, confirming our numerical data in Fig. 8.

Case 4: Realistic experimental data for carbon nanotube fibers and copper

We apply our theory to two examples, carbon nanotube fibers (CNFs) and copper, with realistic temperature dependent electrical conductivity $\sigma(T)$ and thermal conductivity $\kappa(T)$ taken from experimental measurements. For CNFs, we use $\sigma(T)$ and $\kappa(T)$ from Fig. 3 of Ref. 17 (samples A, B, and C). The data are polynomial interpolated, as shown in Figs. 9(a) and 9(b). We then solve Eqs. (5) and (6) numerically. We assume the length of the CNFs is $L = 1\,\mu$m. First, for $T_1 = T_2 = 360\,$K, we calculate the maximum temperature T_{max} as a function of the applied voltage V_0, as shown in Fig. 9(c). We next calculate T_{max} for various T_2, for a fixed bias voltage of $V_0 = 0.63\,$V and $T_1 = 360\,$K, as shown in Fig. 9(d). The results are compared with those obtained for constant electrical and thermal conductivities, $\sigma(T) = \sigma_0 = \sigma(T = 360\,\mathrm{K})$ and $\kappa(T) = \kappa_0 = \kappa(T = 360\,\mathrm{K})$. The constant σ and κ approximation is fairly close to the actual data, for samples B and C, but not for sample A. This is because both electrical

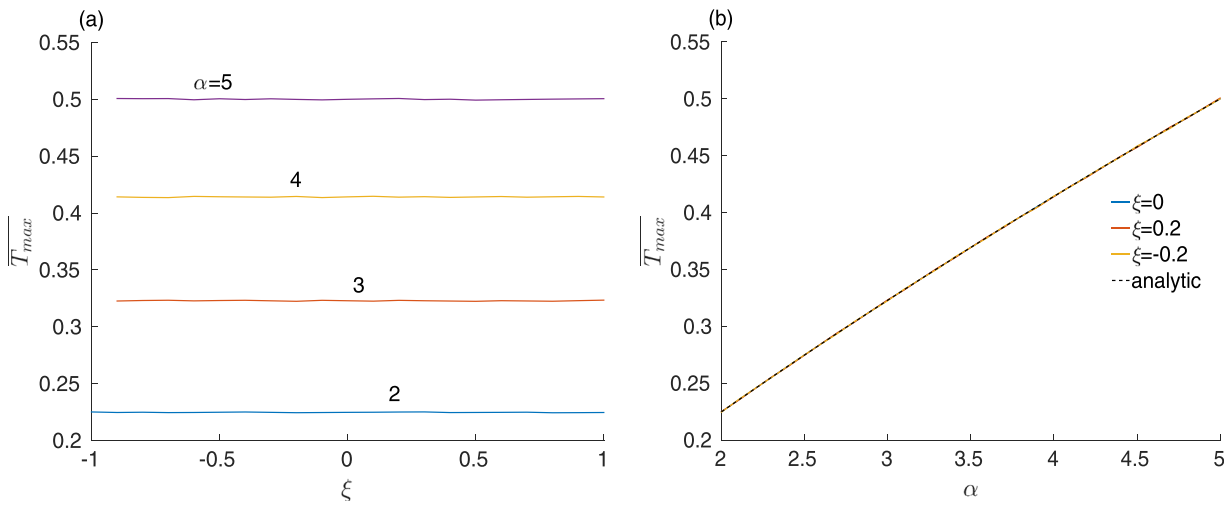

FIG. 8. The maximum temperature (a) as a function of ξ for various values of α; (b) as a function of α for various values of ξ. Solid lines are for numerical calculation from Eqs. (5) and (6); dashed line is for analytical solution, Eq. (13).

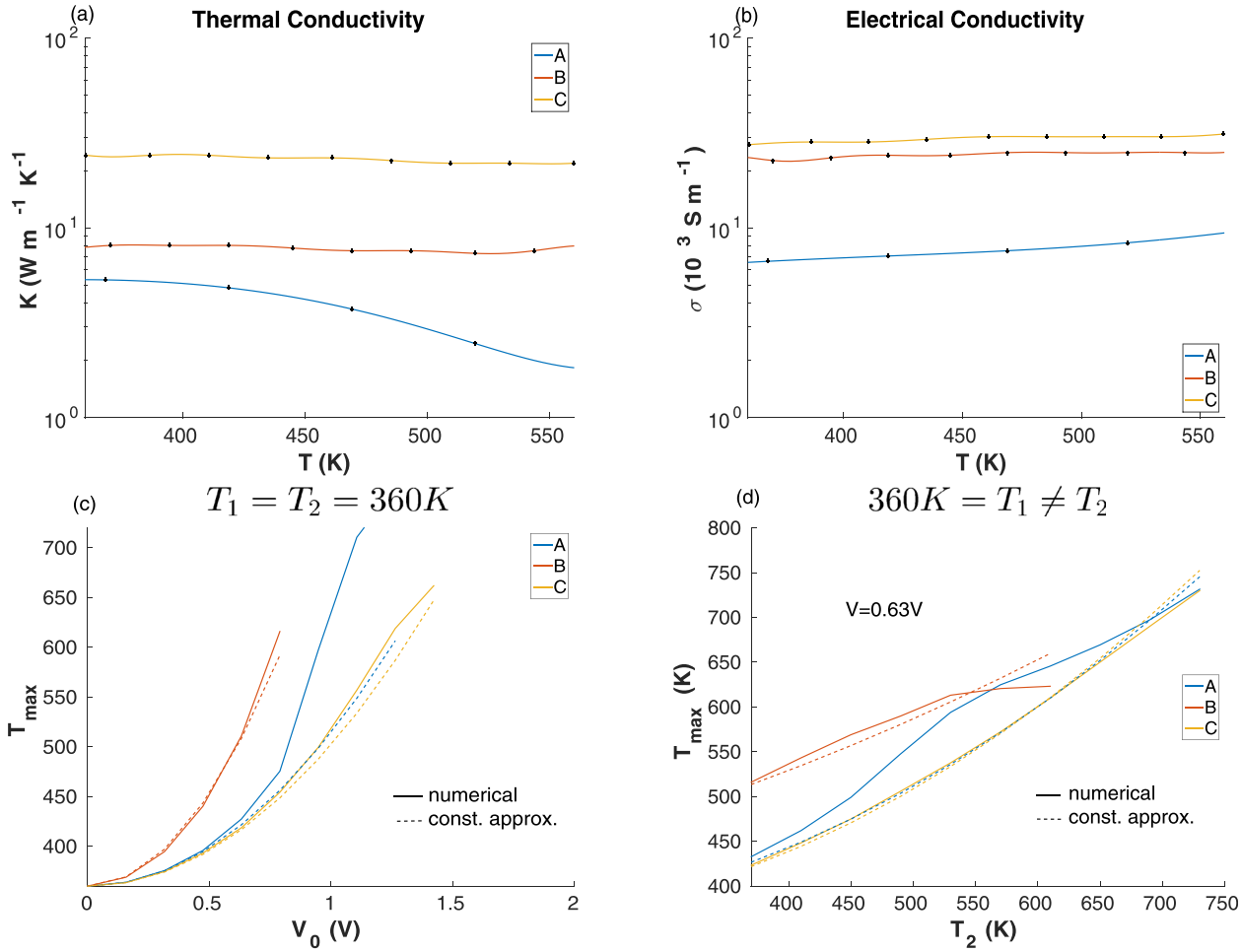

FIG. 9. Carbon nanotube fibers (CNFs). (a) Thermal conductivity $\kappa(T)$ and (b) electrical conductivity $\sigma(T)$ taken from samples A-C in Fig. 3 of Ref. 17. Lines in (a) and (b) are polynomial fits to the data points. (c) T_{max} as a function of V_0, for $T_1 = T_2 = 360$ K. (d) T_{max} as a function of T_2, for $V_0 = 0.63$ V and $T_1 = 360$ K. In (c) and (d), we assume $L = 1$ μm; solid lines are for numerical calculation using $\kappa(T)$ and $\sigma(T)$ in (a) and (b), and dashed lines are for the constant approximation conductivities, $\sigma(T) = \sigma(T = 360\,\mathrm{K})$ and $\kappa(T) = \kappa(T = 360\,\mathrm{K})$.

and thermal conductivities are close to constant for cases B and C in Figs. 9(a) and 9(b). For sample A, σ increases and κ decreases with temperature T. As a result, the rate of Joule heating would increase faster than that of thermal conduction, resulting in a larger T_{max} in the conductor than that with constant conductivities. Noticeably, among the three samples, sample A had the weakest nanotube fiber alignment, the least emission current, the largest turn on voltage for field emission, and the smallest field enhancement factor.[17] Note that our calculation has ignored the radiative losses from the walls of the carbon nanotubes.[31–33]

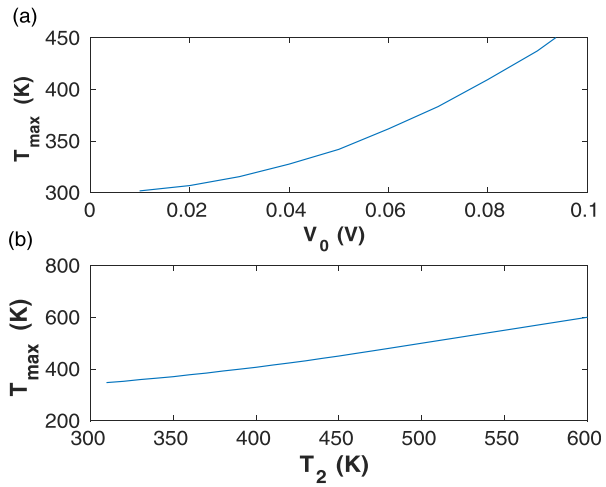

FIG. 10. Copper with WF law. (a) T_{max} as a function of V_0, for $T_1 = T_2 = 300$ K. (b) T_{max} as a function of T_2, for $V_0 = 0.63$ V and $T_1 = 300$ K. $L = 1$ μm is assumed in the calculations.

For copper, we adopt the WF law. As discussed in Case 3 above, T_{max} can be found without knowing the detailed temperature of $\sigma(T)$ and $\kappa(T)$. For $T_1 = T_2 = 300$ K, the temperature of the electrical conductivity of copper[34] gives $\xi = -0.58$. Figure 10(a) shows the resulting maximum temperature T_{max} as a function of the applied voltage V_0, for $T_1 = T_2 = 300$ K. Figure 10(b) shows T_{max} as a function of T_2, for a fixed bias voltage of $V_0 = 0.63$ V and $T_1 = 300$ K.

IV. SUMMARY

In this paper, we evaluate the effects of temperature dependence of the electrical and thermal conductivities on the Joule heating of a one-dimensional conductor, by solving the coupled non-linear steady state electrical and thermal conduction equations. We found that there are conditions under which no steady state solution exists. In the special case of

constant electrical conductivity and linear temperature dependence of the thermal conductivity, we have obtained explicit expressions for the bounds of existence of solutions. The shifting of these bounds due to the introduction of linear temperature dependence of electrical conductivity is also examined. The temperature distribution, the maximum temperature, and its location within the conductor are examined for various boundary conditions. Sample calculations for carbon nanotube fibers and copper are demonstrated. We note that the absence of a steady state solution may indicate the occurrence of thermal runaway. This may be a topic for future research. Additional topics include the stability of the steady state and the effects of thermal insulation (zero heat flux boundary condition) imposed on one end of the sample. So far, the role of the boundaries or thermal contacts has not been discussed in this paper. There should be some temperature jumps at the thermal contacts, with coupling between electrical and thermal transport, see, e.g., Ref. 35. These couplings should also play a role in the steady state temperature profile, which will be studied in the future.

ACKNOWLEDGMENTS

This work was supported by the AFOSR Grant No. FA9550-14-1-0309 and by the L-3 Communications Electron Device Division. PZ was also supported by AFOSR through a subcontract from the University of Michigan.

APPENDIX: DERIVATION OF $\overline{T_{max}}$ WHEN WIEDEMANN-FRANZ LAW HOLDS

For the Wiedemann-Frantz law holding, with $T_1 = T_2$ we have $\alpha = V_0^2/\tau L T_1$, $\bar{\sigma}(0) = \bar{\sigma}(1) = 1$, $\bar{T}(0) = \bar{T}(1) = 0$. Due to symmetry, the maximum temperature occurs at $\bar{z} = 0.5$, $\bar{T}(0.5) = \overline{T_{max}}$, $\frac{d\bar{T}}{d\bar{z}}|_{0.5} = 0$. We have

$$\bar{K} = \bar{\sigma}(1 + \bar{T}), \tag{A1}$$

$$\frac{d}{d\bar{z}}\left(\bar{K}\frac{d\bar{T}}{d\bar{z}}\right) = -\alpha\frac{\bar{J}^2}{\bar{\sigma}}, \tag{A2}$$

$$\int_0^1 \frac{J}{\bar{\sigma}} d\bar{z} = 1. \tag{A3}$$

Integrating (A2) from 0 to 1 with respect to $\bar{z}$ and using (A3) for the right hand side, we get

$$\bar{K}(1)\frac{d\bar{T}}{d\bar{z}}\bigg|_1 - \bar{K}(0)\frac{d\bar{T}}{d\bar{z}}\bigg|_0 = -\alpha\bar{J}.$$

Since $\bar{K}(0) = \bar{K}(1) = 1$ and because of symmetry $\frac{d\bar{T}}{d\bar{z}}|_1 = -\frac{d\bar{T}}{d\bar{z}}|_0$, we get

$$\frac{d\bar{T}}{d\bar{z}}\bigg|_0 = \frac{\alpha\bar{J}}{2}.$$

Now multiplying (A2) by $(1 + \bar{T})\bar{\sigma}\frac{d\bar{T}}{d\bar{z}}$ and integrating, we get

$$\frac{1}{2}\left((1 + \bar{T})\bar{\sigma}\frac{d\bar{T}}{d\bar{z}}\right)^2 = -\alpha\bar{J}^2\left(\bar{T} + \frac{\bar{T}^2}{2}\right) + c.$$

For $\bar{z} = 0.5$, since $\frac{d\bar{T}}{d\bar{z}} = 0$, so we get $c = \alpha\bar{J}^2(\overline{T_{max}} + \frac{\overline{T_{max}}^2}{2})$. Plugging in $\bar{z} = 0$ in the above equation yields

$$\frac{1}{2}\left(\frac{d\bar{T}}{d\bar{z}}\bigg|_0\right)^2 = \alpha\bar{J}^2\left(\overline{T_{max}} + \frac{\overline{T_{max}}^2}{2}\right),$$

$$\frac{\alpha^2\bar{J}^2}{4} = \alpha\bar{J}^2\left(2\overline{T_{max}} + \overline{T_{max}}^2\right),$$

$$\left(\overline{T_{max}} + 1\right)^2 = \frac{\alpha}{4} + 1,$$

$$\overline{T_{max}} = \pm\sqrt{\frac{\alpha}{2} + 1} - 1.$$

For $\alpha = 0$, we should have $\overline{T_{max}} = 0$ so the $(+)$ sign is chosen. Therefore, we obtain

$$\overline{T_{max}} = \sqrt{\frac{\alpha}{4} + 1} - 1, \tag{A4}$$

which is Eq. (13) in the main text.

[1]M. R. Gomez, J. C. Zier, R. M. Gilgenbach, D. M. French, W. Tang, and Y. Y. Lau, Rev. Sci. Instrum. **79**, 93512 (2008).
[2]L. de' Medici, Phys. Rev. Appl. **5**, 24001 (2016).
[3]P. Zhang, Y. Y. Lau, and R. M. Gilgenbach, J. Appl. Phys. **105**, 114908 (2009).
[4]C. Pérez-Arancibia, P. Zhang, O. P. Bruno, and Y. Y. Lau, J. Appl. Phys. **116**, 124904 (2014).
[5]R. Holm, *Electric Contacts: Theory and Application*, 4th ed. (Springer, Berlin, New York, 1967).
[6]R. S. Timsit and A. Luttgen, Appl. Phys. Lett. **108**, 121603 (2016).
[7]P. Zhang and Y. Y. Lau, J. Appl. Phys. **108**, 44914 (2010).
[8]P. Zhang, Y. Y. Lau, and R. M. Gilgenbach, J. Appl. Phys. **109**, 124910 (2011).
[9]P. Zhang, Y. Y. Lau, and R. M. Gilgenbach, J. Phys. Appl. Phys. **48**, 475501 (2015).
[10]D. D. Ryutov, M. S. Derzon, and M. K. Matzen, Rev. Mod. Phys. **72**, 167 (2000).
[11]M. Pedram and S. Nazarian, Proc. IEEE **94**, 1487 (2006).
[12]H. Kam, E. Alon, and T.-J. K. Liu, IEEE Int. Electron Devices Meet. **2010**, 16.4.1–16.4.4.
[13]P. Zhang, Y. Y. Lau, and R. S. Timsit, IEEE Trans. Electron Devices **59**, 1936 (2012).
[14]D. Shiffler, T. K. Statum, T. W. Hussey, O. Zhou, and P. Mardahl, in *Modern Microwave and Millimeter Wave Power Electronics* (IEEE, Piscataway, NJ, 2005), p. 691.
[15]G. S. Bocharov and A. V. Eletskii, Tech. Phys. **52**, 498 (2007).
[16]W. Tang, D. Shiffler, K. Golby, M. LaCour, and T. Knowles, J. Vac. Sci. Technol. B **30**, 61803 (2012).
[17]S. B. Fairchild, J. Boeckl, T. C. Back, J. B. Ferguson, H. Koerner, P. T. Murray, B. Maruyama, M. A. Lange, M. M. Cahay, N. Behabtu, C. C. Young, M. Pasquali, N. P. Lockwood, K. L. Averett, G. Gruen, and D. E. Tsentalovich, Nanotechnology **26**, 105706 (2015).
[18]D. P. Hunley, S. L. Johnson, R. L. Flores, A. Sundararajan, and D. R. Strachan, J. Appl. Phys. **113**, 234306 (2013).
[19]S. Hertel, F. Kisslinger, J. Jobst, D. Waldmann, M. Krieger, and H. B. Weber, Appl. Phys. Lett. **98**, 212109 (2011).
[20]M.-H. Bae, Z.-Y. Ong, D. Estrada, and E. Pop, Nano Lett. **10**, 4787 (2010).
[21]Q. Ma, N. M. Gabor, T. I. Andersen, N. L. Nair, K. Watanabe, T. Taniguchi, and P. Jarillo-Herrero, Phys. Rev. Lett. **112**, 247401 (2014).
[22]K. Kuribara, H. Wang, N. Uchiyama, K. Fukuda, T. Yokota, U. Zschieschang, C. Jaye, D. Fischer, H. Klauk, T. Yamamoto, K. Takimiya, M. Ikeda, H. Kuwabara, T. Sekitani, Y.-L. Loo, and T. Someya, Nat. Commun. **3**, 723 (2012).
[23]M. J. Kang, E. Miyazaki, I. Osaka, K. Takimiya, and A. Nakao, ACS Appl. Mater. Interfaces **5**, 2331 (2013).
[24]J. Shane, Q. Gu, F. Vallini, B. Wingad, J. S. T. Smalley, N. C. Frateschi, and Y. Fainman, Proc. SPIE **8980**, 898027 (2014).

[25]P. Zhang, Q. Gu, Y. Y. Lau, and Y. Fainman, IEEE J. Quantum Electron. **52**, 2000207 (2016).
[26]Y. Y. Lau, D. Chernin, P. Zhang, and R. M. Gilgenbach, "A voltage scale for electro-thermal runaway," in *2013 19th IEEE Pulsed Power Conference PPC* (2013), pp. 1–2.
[27]N. W. Ashcroft and N. D. Mermin, *Solid State Physics*, 1st ed. (Brooks Cole, New York, 1976).
[28]E. Pop, D. A. Mann, K. E. Goodson, and H. Dai, J. Appl. Phys. **101**, 93710 (2007).
[29]T. Y. Kim, C.-H. Park, and N. Marzari, Nano Lett. **16**, 2439 (2016).
[30]N. Wakeham, A. F. Bangura, X. Xu, J.-F. Mercure, M. Greenblatt, and N. E. Hussey, Nat. Commun. **2**, 396 (2011).
[31]S. T. Purcell, P. Vincent, C. Journet, and V. T. Binh, Phys. Rev. Lett. **88**, 105502 (2002).
[32]P. Vincent, S. T. Purcell, C. Journet, and V. T. Binh, Phys. Rev. B **66**, 75406 (2002).
[33]J. A. Sanchez, M. P. Menguc, K. F. Hii, and R. R. Vallance, J. Thermophys. Heat Transfer **22**, 281 (2008).
[34]R. A. Matula, J. Phys. Chem. Ref. Data **8**, 1147 (1979).
[35]J. Lombard, F. Detcheverry, and S. Merabia, J. Phys.: Condens. Matter **27**, 15007 (2015).